Sci. Technol. Adv. Mater. **10** (2009) 065001 (6pp) doi:10.1088/1468-6996/10/6/065001

Fabrication and characteristics of porous germanium films

Chengbin Jing[1,2], Chuanjian Zhang[1], Xiaodan Zang[1], Wenzheng Zhou[2], Wei Bai[2], Tie Lin[2] and Junhao Chu[2]

[1] College of Materials Science and Technology, Qingdao University of Science and Technology, 53 Zheng-zhou Road, Qingdao 266042, People's Republic of China
[2] National Laboratory for Infrared Physics, Shanghai Institute of Technical Physics, Chinese Academy of Sciences, Shanghai 200083, People's Republic of China

E-mail: jingchngbin0028@sina.com

Received 14 August 2009
Accepted for publication 19 November 2009
Published 29 December 2009
Online at stacks.iop.org/STAM/10/065001

Abstract
Porous germanium films with good adhesion to the substrate were produced by annealing GeO_2 ceramic films in H_2 atmosphere. The reduction of GeO_2 started at the top of a film and resulted in a Ge layer with a highly porous surface. TEM and Raman measurements reveal small Ge crystallites at the top layer and a higher degree of crystallinity at the bottom part of the Ge film; visible photoluminescence was detected from the small crystallites. Porous Ge films exhibit high density of holes (10^{20} cm^{-3}) and a maximum of Hall mobility at ~225 K. Their p-type conductivity is dominated by the defect scattering mechanism.

Keywords: germanium, porous structured film, visible photoluminescence, semiconducting behavior

1. Introduction

Porous semiconductor materials with visible photoluminescence (PL) are a topic of intense interest owing to their unique optoelectronic and morphological properties, as well as biocompatibility characteristics [1–4]. In the last decade, most research efforts have concentrated on porous silicon [4–6]. Germanium is another important group IV semiconductor with similar properties to Si. It has a potential to replace Si in advanced integrated optoelectronic devices because of its higher mobility of holes and electrons, smaller band gap, larger effective Bohr radius (24 nm at 300 K), and higher solubility of dopants [7–10]. The work on porous Ge is limited by the lack of adequate procedures for its fabrication [2, 3]. It has been particularly challenging to synthesize group IV materials, such as Si and Ge, primarily owing to their strong covalent bonding and the need for high temperatures to promote crystallization [11–13]. Anodization and electrochemical etching [3, 14–18], spark processing [19, 20] and inductively coupled plasma chemical vapor deposition (ICPCVD) [2, 21] have been used to prepare porous Ge films. It is still a challenge to produce porous, semiconducting and luminescent Ge films in a simple and robust way, allowing their subsequent processing and integration into working devices [1–3, 14–20]. The porous structure plays an important role in the visible PL emission of the indirect bandgap semiconductors, such as Si and Ge [4–6, 14–20]. Formation of porous structures likely enhances electrical resistivity and carrier scattering rate, hindering measurements of the transport properties; it also may decrease the adhesion between the film and substrate. These factors may limit the use of the porous films.

In this paper, we report a simple route for preparing Ge films with a good adhesion to the substrate, highly porous surface layer and a denser bottom part of the film. Visible PL and the carrier transport characteristics were measured and discussed in terms of the morphology and sample structure.

2. Experimental details

All chemicals used in this study were of analytical purity. GeO_2 ceramic films were prepared based on previous studies [22–24]. Five grams of hexagonal crystalline GeO_2 powder (99.9999%) was mixed with 100 ml of aqueous

ammonia (6 M) in a glass beaker. After stirring at 50 °C for 40 min, a transparent solution was obtained. The pH value of the solution was adjusted to 2 using acetic acid. Soda-lime-silica glass slides were cleaned ultrasonically in acetone and deionized water for 30 and 40 min, respectively, and were placed vertically into the glass beaker. White GeO_2 ceramic films were gradually grown on the substrate via a liquid phase deposition (LPD) at room temperature. They were washed in deionized water, dried at 50 °C for 1 h, and annealed at 550 °C for 5–120 min in H_2 atmosphere (0.1 MPa). GeO_2 can be thermally (500–700 °C) reduced with hydrogen gas to metallic Ge. Since the soda-lime-silica glass slide might deform at above 600 °C, the lower temperature of 550 °C was used for thermal reduction of GeO_2.

The crystallinity of the films was confirmed by x-ray diffraction (XRD, D8 Advance). Morphology observations were carried out on the gold-coated samples using a scanning electron microscope (FE-SEM, JSM-6700F). Adhesion was measured by the tape test (ASTM D3359). A grating pattern with 11 cuts in x and y directions was carved in the film down to the substrate. Pressure-sensitive tape was applied over the grating and then removed, and the number of peeled-off segments was counted. Adhesion was assessed on a 0 to 5 B scale according to the percentage of those segments, namely 0 B ($>$ 65%), 1 B (35–65%), 2 B (15–35%), 3 B (5–15%), 4 B ($<$ 5%), and 5 B (0% or none).

For high-resolution transmission electron microscopy observations (HRTEM, JEM-2010F), a piece of a 12 μm thick Ge film was carefully peeled off the glass substrate with a knife. This sample was further sectioned using an ultramicrotome (RMC MTXL, USA). Electron beam induced crystallization of the sample was not observed during the HRTEM observations.

Room-temperature micro-Raman measurements were performed with a Renishaw Raman system using a 325 nm laser excitation. The laser spot size on the sample was 1–2 μm. The laser power was 6 mW and the laser-induced heating of the sample is negligible. PL spectra were recorded at room temperature with a Hitachi 850 fluorescence spectrophotometer equipped with a xenon lamp. Excitation wavelength was 375 nm.

Carrier transport was examined using Hall effect measurements. Indium contacts were deposited onto the film surface in the Van der Pauw geometry. They were annealed at a temperature above the melting point of indium (300 °C) for 15 min under argon atmosphere. Copper wires were soldered to the indium contact pads. In this procedure, indium could penetrate the porous surface layer and contact the bottom part of the film. The Ohmic nature of the contacts was confirmed over the entire studied temperature range through the symmetrical and linear I–V characteristics.

3. Results and discussions

3.1. X-ray diffraction

Figure 1 shows the XRD patterns of the LPD GeO_2 film and the GeO_2 films annealed at 550 °C for 5, 60 and 120 min under H_2 atmosphere. The LPD GeO_2 film has a hexagonal crystal structure (ICDD-PDF No: 36-1463). It was transformed into a Ge film with cubic structure (ICDD-PDF No: 65-0333) after annealing for 120 min. Peaks corresponding to tetragonal GeO_2 are observed in the XRD pattern of the film annealed for 5 or 60 min, showing that partially hexagonal GeO_2 was transformed into tetragonal GeO_2 during the annealing. It is known that hexagonal GeO_2 is metastable and can transform into tetragonal GeO_2 under atmospheric annealing [25, 26]. The well-known reduction reaction [26, 27] took place during annealing, converting GeO_2 into cubic Ge as shown in figure 1.

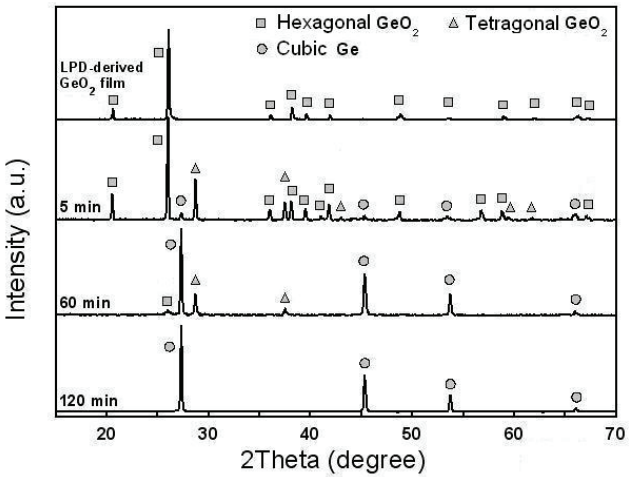

Figure 1. XRD patterns of LPD GeO_2 film before and after annealing for 5, 60 and 120 min under H_2 atmosphere.

$$GeO_2 + 2H_2 \xrightarrow{\text{heating}} Ge + 2H_2O. \quad (1)$$

3.2. Electron microscopy

Figure 2 presents SEM images of GeO_2 films: initial (a, b) and annealed for 5 min (c, d) and 120 min (e, f) under H_2 atmosphere. Figures 2(a) and (b) reveal that the LPD GeO_2 film is compact and has a rough surface. Annealing for 5 min produced numerous small pores (figure 2(c)). The cross-sectional image of the film (see figure 2(d)) reveals that the pores were formed in the top surface layer and thus the reduction of GeO_2 started from the top of the film. A film with an interconnected, sponge-like structure and a window size of about 500 nm to 1 μm in the top surface layer (about 3 μm thickness) was produced after annealing for 120 min (see figures 2(e) and (f)). The film has a thickness of 12 μm. Its bottom part is thicker (about 9 μm) and denser than the top surface layer, resulting in good adhesion to the substrate ($\geqslant$ 4 B as determined by the adhesion measurement, ASTM D 3359). As shown by reaction (1), the reduction of GeO_2 is combined with the release of water. The reduction of GeO_2 progressed from the top to the bottom part of the film, and the water vapors produced inside continuously penetrated the film. This likely generated porosity, especially in the top layers.

Figure 3 displays typical HRTEM lattice fringe images, as well as fast Fourier transforms (FFT) patterns of the

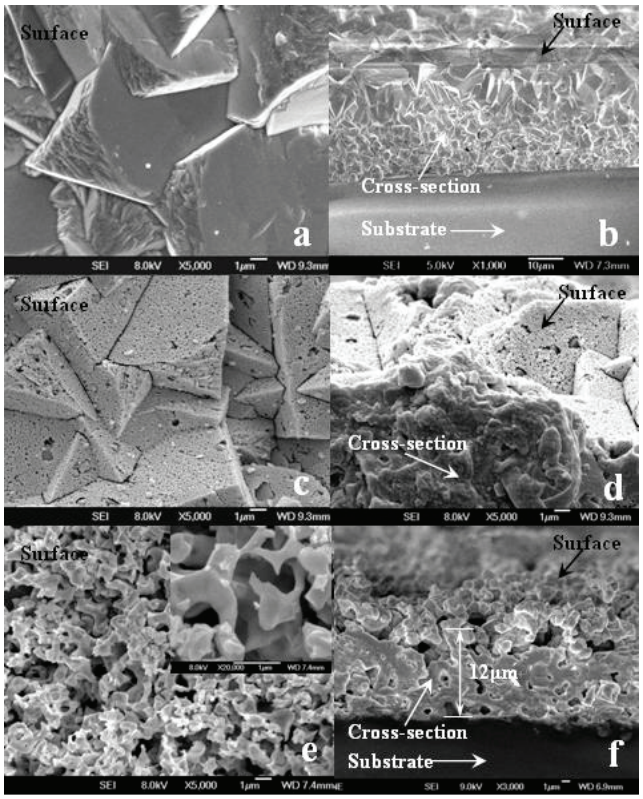

Figure 2. SEM images of LPD GeO_2 film before (a, b) and after annealing for 5 (c, d) and 120 min (e, f) under H_2 atmosphere.

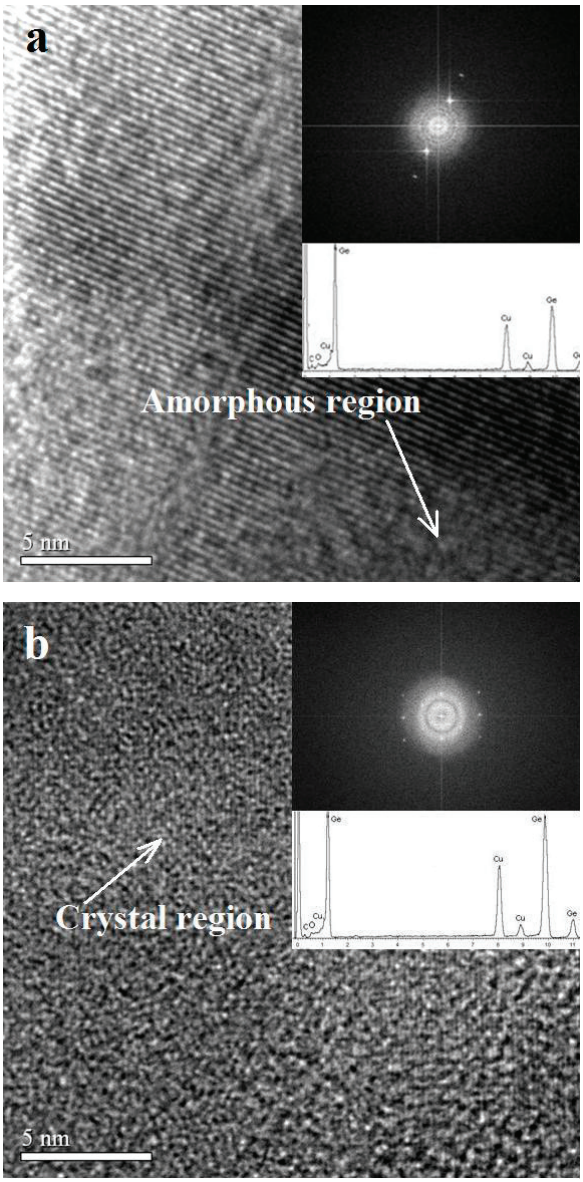

Figure 3. HRTEM images of the bottom part (a) and top surface layer (b) of the GeO_2 film annealed for 120 min. Insets are the FFT patterns and the energy dispersive x-ray spectra.

bottom part (figure 3(a)) and top surface layer (figure 3(b)) of the GeO_2 film annealed for 120 min. Figures 3(a) and (b) reveal that the degree of crystallinity at the bottom part is higher than that at the top part of the film. A few small amorphous regions in figure 3(a) (marked by the arrow) imply that the bottom part did not crystallize completely. Figure 3(b) reveals that small crystallites exist in the top surface layer (as indicated by the arrow). The fast Fourier transforms pattern (inset of figure 3(b)) features a combination of spots from a crystalline phase and halos from an amorphous phase. Ge, Cu, C and O were detected in the film by energy dispersive x-ray spectroscopy (EDS, see insets of figures 3(a) and (b)). Copper, carbon, and partly oxygen, originated from the sample support.

3.3. Raman scattering

We have analyzed the film samples and the substrate by micro-Raman spectroscopy. Curves a and b in figure 4 are Raman spectra detected from the surface and cross-section (the bottom part) of the GeO_2 film annealed for 120 min, respectively. Curve c is the Raman spectrum of the glass substrate; it differs significantly from spectra a and b. The use of short-wavelength excitation (325 nm) and 12-μm-thick film enabled measurement of the Raman signal from the top layer without significant contribution from the underlying substrate [28] (spectra a and b). Ge–O and Ge–O–Ge bonds cause Raman scattering peaks at 211, 246, 262, 327 and 442 cm^{-1} [16, 20]. Such peaks are not observed in spectra a and b, confirming that the film unlikely contains oxygen. The top surface layer and the bottom part of the film exhibit sharp peaks at 295 and 299 cm^{-1}, respectively. A wide tail is visible at the low-frequency side of the 295 cm^{-1} peak; this tail is much shorter for the 299 cm^{-1} peak. Noting that amorphous Ge exhibits a wide Raman band centered at about 275 cm^{-1} [20], the top surface layer should contain much more amorphous Ge phases compared with the bottom part. This conclusion is consistent with HRTEM (see figure 3). The first-order Ge–Ge optical phonon of single-crystal Ge exhibits a sharp Raman peak at 300 cm^{-1} [18, 29]. The Ge–Ge Raman peak of the top surface layer shifts 5 cm^{-1} towards lower frequency, whereas the shift is only about 1 cm^{-1} for the bottom part. Several reasons, such as phonon confinement, stress and polycrystallinity, can shift the Ge–Ge optical phonons [30, 31]. Compressive stress leads to an upward shift of the Ge–Ge mode, while

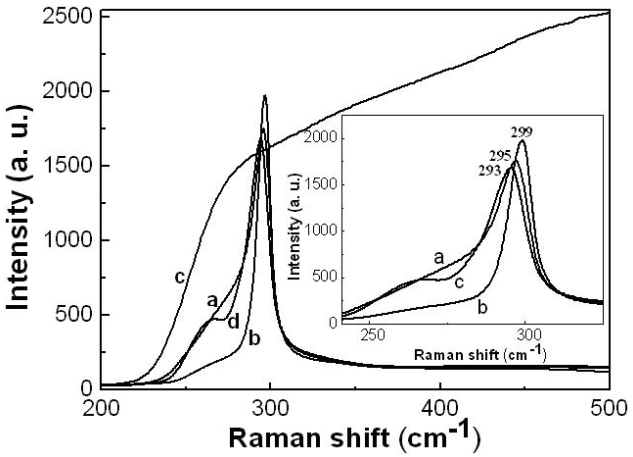

Figure 4. Raman spectra of the films (a, b, d) and the glass substrate (c). Curves a and b correspond to the surface and the cross-section (the bottom part) of the GeO_2 film annealed for 120 min, respectively. Spectrum c was recorded from the substrate surface, and curve d from the surface of the porous Ge film annealed at 550 °C for 30 min.

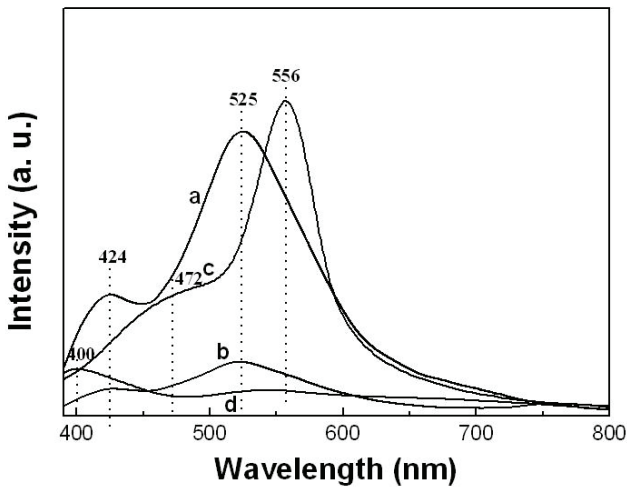

Figure 5. PL spectra of the film (a, b, and c) and the glass substrate (d). Curves a, b, and c are PL spectra of the GeO_2 films annealed for 0, 60 and 120 min, respectively. All spectra were detected from the sample surfaces.

phonon confinement and tensile stress lead to a downward shift [32–34, 35]. As for polycrystallinity, it may result in inhomogeneous broadening (with low frequency tailing) and minor peak shifts [31, 36, 37]. The effect of stress on Raman shift can be changed by stress relaxation using post-annealing [38–40]. For instance, the Raman peak of a Ge sample with compressive strain shifts to lower frequencies as the annealing time increases [32, 41, 42]. This phenomenon was also observed in this study. We annealed a porous Ge film at 550 °C for 30 min and recorded its Raman spectrum from the film surface. The result (curve *d* in figure 4) illustrates that the Ge–Ge Raman peak is shifted downward by about 2 cm^{-1}. The compressive strain in the top surface layer relaxes with increasing annealing time, and thus the phonon confinement effects become relatively more evident, causing the shift of the observed peak. After post-annealing, the tail-like band shown in curve a changes into a wide peak (curve d) that has been observed in Raman spectra of various Ge nanostructures [18, 30, 32, 43]. This implies that the wide tail-like band shown in spectrum a is unlikely caused by the polycrystallinity. Before post-annealing, the downward Raman shift caused by phonon confinement is masked to some degree by the upward Raman shift due to compressive stress. This masking effect may produce a wide tail-like band [44]. The phonon confinement causes a larger Raman shift in comparison with the compressive stress. This leads us to consider that the phonon confinement effect plays a more important role in the Raman peak shift shown by spectrum a. Curve b has a short low-frequency tail and a minor peak shift (about 1 cm^{-1}), probably caused by the polycrystallinity. Post-annealing had little effect on the shape and position of the Raman peak of the bottom part of the film. This demonstrates that polycrystallinity might have been previously achieved in this part. It is known that the stress declines with increasing film thickness due to stress relief during grain growth [45]. The bottom part of the film is about 9-μm-thick and has a higher degree of crystallinity. Stress in this part should be rather small. Raman shift caused by stress relaxation after post-annealing may not be clearly observed in the Raman spectrum of this part.

3.4. Photoluminescence

Curves a, b and c in figure 5 show PL spectra of the GeO_2 films annealed for 0, 60 and 120 min, respectively. Curve d corresponds to the glass substrate. All these PL spectra were detected from the sample surfaces. The substrate exhibits a weak PL peak at 400 nm (see curve d). Germanium oxides show two bands centered at around 3.1 and 2.2 eV, respectively [46, 47]. The peaks at 424 and 525 nm (curve a) can be ascribed to the Ge oxides; these two peaks decreased upon annealing (see curve b). This is consistent with the previous observation that 400 and 564 nm PL bands decreased with the decreasing O/Ge ratio [48]. After annealing for 120 min, the sample exhibits PL bands at 472 and 556 nm (see curve c). These two peaks overlap considerably and form a broad band within the wavelength range 400–620 nm. The shape and position of this band are quite different from those of the PL band in spectra a and b. If this broad PL band resulted from Ge oxides it would be much weaker than that of the PL band in spectrum b, because the O/Ge ratio of the film annealed for 120 min should be much lower than that of the film annealed for 60 min. Evidently, this is not the case in figure 5. Existence of Ge oxides was not supported by Raman analysis and thus the broad PL band in spectrum c unlikely originates from those. Ge and Si are typical indirect bandgap semiconductors that do not emit visible light [4–6]. If nanostructures formed in these materials, visible PL emission would be possible due to the quantum confinement effect [14–20, 49, 50]. The PL band observed in spectrum c hardly resulted from the bottom part of the film. The bottom part of the film has a higher degree of crystallinity and its average crystallite size (about 38 nm, as determined by HRTEM) is larger than the effective Bohr radius for Wannier excitons in Ge (24 nm, 300 K). HRTEM and Raman

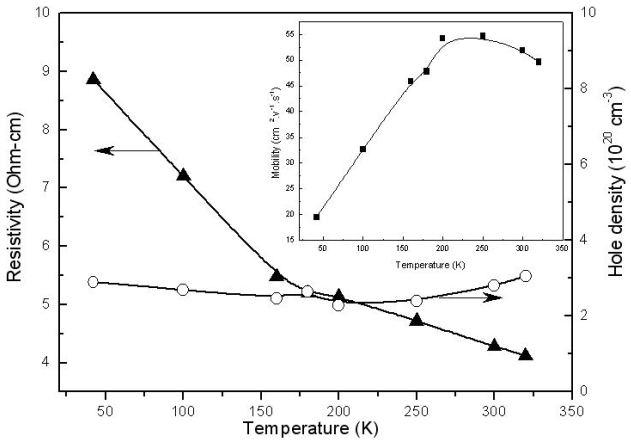

Figure 6. Temperature-dependent electrical resistivity and carrier density of the porous Ge film. The inset shows temperature dependence of carrier mobility.

results suggest that nanometer-sized Ge crystallites exist in the top surface layer of the film. Recombination of excitations confined in these small Ge crystal phases may lead to visible PL. Size distribution in semiconductor quantum dots always broadens PL peaks. The top surface layer of the film contains irregularly shaped and sized Ge crystallites (see figure 3), which might produce the broad PL band of spectrum c.

3.5. Hall effect

Temperature dependences of resistivity and carrier density in the porous Ge film are shown in figure 6. As mentioned in the experimental section, the annealing at 300 °C might induce indium diffusion from the film surface, through the pores, to the bottom part of the film. The latter was much denser and thicker than the top surface layer and therefore could dominate the measured transport properties. The resistivity decreases with increasing temperature over the measured temperature region, revealing semiconducting behavior. At 300 K, the resistivity (4.2 Ω cm) is about 12 times lower than that of pure bulk Ge (50 Ω cm). The conductivity is caused by holes and their density is about 2.8×10^{20} cm^{-3} at 300 K. This density is some seven orders of magnitude higher than that of the pure crystalline Ge (2.4×10^{13} cm^{-3} at 300 K). As our sample was not intentionally doped, the ultra-high hole concentration cannot be accounted for by impurities. Structural defects, such as dangling bonds at the grain boundaries and in dislocation networks can provide Ge film with high density of acceptor levels [51–56]. As shown by SEM, HRTEM and Raman analysis, the film contains porous structures, as well as crystalline and amorphous regions. A large number of structural defects exist in the film, resulting in a high density of holes. Because the density of those structural defects should be unchanged within the studied temperature range, the carrier density of the film varies slightly with increasing temperature (see figure 6).

The inset of figure 6 presents the temperature dependence of carrier mobility in the porous Ge film. The mobility increases with temperature increase from 42 to 225 K and decreases above 225 K. The Hall mobility μ can be expressed as

$$\mu = \frac{q}{m^*} \times \frac{1}{AT^{3/2} + (BN/T^{3/2})}, \tag{2}$$

where q and m^* are charge and effective mass of the carrier, A and B are constants, N is carrier concentration and T is temperature [54]. Numerous structural defects provide the sample with a large N value ($\sim 10^{20}$ cm^{-3}). At low temperature, $BN/T^{3/2}$ can be larger than $AT^{3/2}$ and the mobility μ increases with temperature. At high temperatures, the $AT^{3/2}$ term can exceed $BN/T^{3/2}$ even for large N values, resulting in the mobility decrease with temperature. A maximum should be observed in between, that is about 225 K (see inset of figure 6).

4. Conclusions

Porous Ge film was obtained by annealing LPD GeO_2 film under H_2 atmosphere. The bottom part of the film is denser and thicker than the top surface layer, resulting in good adhesion to the substrate. The top surface layer of the film is highly porous and contains amorphous phases and small crystallites. The quantum confinement effects in those crystallites produces visible photoluminescence within the wavelength range of 400–620 nm. The porous Ge film has a high density of holes (10^{20} cm^{-3}) and exhibits a p-type semiconducting behavior. The Hall mobility peaks at ~225 K and is possibly dominated by the defect scattering mechanisms.

Acknowledgments

This work was financially supported by National Natural Science foundation of China (50802046), National Basic Research Program of China (no. 2007CB924900), National Innovation Research Group foundation of China (no. 60821692) and the Key Project of Shanghai Science and Technology Commission (no. 07JC14018).

References

[1] Sun D, Riley A E, Cadby A J, Richman E K, Korlann S D and Tolbert S H 2006 *Nature* **441** 1126
[2] Shieh J, Chen H L, Ko T S, Cheng H C and Chu T C 2004 *Adv. Mater.* **16** 1121
[3] Choi H C and Buriak J M 2000 *Chem. Commun.* 1669
[4] Sailor M J and Kavanagh K L 1992 *Adv. Mater.* **4** 432
[5] Nakagawa K, Nishida A, Shimada T, Yamaguchi H and Eguchi K 1992 *Japan. J. Appl. Phys.* **31** 515
[6] Collins R T, Fauchet P M and Tischler M A 1997 *Phys. Today* **50** 83
[7] Kodambaka S, Tersoff J, Reuter M C and Ross F M 2007 *Science* **316** 729
[8] Brunco D P 2007 *ECS Trans.* **11** 479
[9] Park Y D, Hanbicki A T, Erwin S C, Hellberg C S, Sullivan J M, Mattson J E, Ambrose T F, Wilson A, Spanos G and Jonker B T 2002 *Science* **295** 651
[10] Adhikari H, Marshall A F, Chidsey C E D and Mclntyre P C 2006 *Nano Lett.* **6** 318
[11] Wang W Z, Poudel B, Huang J Y, Wang D Z, Kunwar S and Ren Z F 2005 *Nanotechnology* **16** 1126

[12] Warner J H, Djouahra S and Tilley R D 2006 *Nanotechnology* **17** 3035
[13] Louisa J and Hope-Weeks 2005 *Chem. Lett.* **34** 1526
[14] Miyazaki S, Sakamoto K, Shiba K and Hirose M 1995 *Thin Solid Films* **255** 99
[15] Flamand G, Poortmans J and Dessein K 2005 *Phys. Status Solidi* C **2** 3243
[16] Kartopu G, Karavanskii V A, Serincan U, Turan R, Hummel R E, Ekinci Y, Gunnæs A and Finstad T G 2005 *Phys. Status Solidi* A **202** 1472
[17] Lomov A A, Bushuev V A, Karavanskii V A and Bayliss S 2003 *Crystallogr. Rep.* **48** 326
[18] Kartopu G, Sapelkin A V, Karavanskii V A, Serincan U and Turan R 2008 *J. Appl. Phys.* **103** 1135181
[19] Chang S S and Hummel R E 2000 *J. Lumin.* **86** 33
[20] Kartopu G, Bayliss S C, Hummel R E, Ekinci Y and Chang S S 2004 *J. Appl. Phys.* **95** 3466
[21] Ko T S, Shieh J, Yang M C, Lu T C, Kuo H C and Wang S C 2008 *Thin Solid Films* **516** 2934
[22] Jing C B, Hou J X, Xu X G and Zhang Y H 2008 *Appl. Phys. A: Mater. Sci. Process.* **90** 367
[23] Jing C B, Hou J X and Zhang Y H 2008 *J. Crystal Growth* **310** 391
[24] Jing C B, Hou J X and Zhang Y H 2007 *J. Am. Ceram. Soc.* **90** 3646
[25] Micoulaut M, Cormier L and Henderson G S 2006 *J. Phys. Condens. Matter* **18** 753
[26] Johnson O H 1952 *Chem. Rev.* **51** 431
[27] Yoshida N, Naknishi M, Ikegami K, Shimura S and Kishimoto S 1987 *J. Mater. Sci. Lett.* **6** 149
[28] Danesh P, Pantchev B, Savatinova I, Liarokapis E and Raptis Y S 1991 *J. Appl. Phys.* **69** 7656
[29] Tu C H, Chang T C, Liu P T, Yang T H, Zan H W and Chang C Y 2006 *Surf. Coat. Technol.* **200** 3261
[30] Liu J L, Wan J, Jiang Z M, Khitun A, Wang K L and Yu D P 2002 *J. Appl. Phys.* **92** 6804
[31] Lien S Y, Mao H Y, Wu B R, Horng R H and Wu D S 2007 *Chem. Vapor Depos.* **13** 247
[32] Liu J L, Jin G, Tang Y S, Luo Y H, Wang K L and Yu D P 2000 *Appl. Phys. Lett.* **76** 586
[33] Fukata N, Oshima T, Murakami K, Kizuka T, Tsurui T and Ito S 2005 *Appl. Phys. Lett.* **86** 213112
[34] Buca D, Holländer B, Trinkaus H, Mantl S, Carius R, Loo R, Caymax M and Schaefer H 2004 *Appl. Phys. Lett.* **85** 2499
[35] Teixeira R C, Doi I, Zakia M B P, Diniz J A and Swart J W 2004 *Mater. Sci. Eng.* B **112** 160
[36] Okada T 1984 *Solid State Commun.* **49** 809
[37] Iqbal Z 1981 *Solid State Commun.* **37** 993
[38] Huang W P, Cheng H H, Sun G, Lou R F, Yeh J H and Shen T M 2007 *Appl. Phys. Lett.* **91** 142102
[39] Iqbal Z and Veprek S 1982 *J. Phys. C; Solid State Phys.* **15** 377
[40] Osten H J, Bugiel E, Dietrich B, Fischer G G, Kim M, Kruger D, Zaumseil P and Endisch D 1996 *Semicond. Sci. Technol.* **11** 1678
[41] Cai Q J, Zhou H and Lu F 2007 *Appl. Surf. Sci.* **253** 4792
[42] Sharp I D *et al* 2005 *Appl. Phys. Lett.* **86** 063107
[43] Dřínek V, Šubrt J, Klementová M, Rieder M and Fajgar R 2009 *Nanotechnology* **20** 035606
[44] Xu X X, Lin H B, Wu Z C, Li H B and Zhang C Z 2002 *Proc. SPIE.* **4923** 164
[45] Fang Z J, Xia Y B, Wang L J and Wang Z M 2002 *J. Phys. Condens. Matter* **14** 5271
[46] Madon M, Gillet P, Julien C and Price G D 1991 *Phys. Chem. Minerals* **18** 7
[47] Zyubin A S, Mebel A M and Lin S H 2006 *J. Chem. Phys.* **125** 064701
[48] Zacharias M and Fauchet P M 1997 *Appl. Phys. Lett.* **71** 380
[49] Maeda Y 1995 *Phys. Rev.* B **51** 1658
[50] Bachrach-Ashkenasy N, Kronik L, Shapira Y, Rosenwaks Y, Hanna M C, Leibovitch M and Ram P 1996 *Appl. Phys. Lett.* **68** 879
[51] Lee H J, Lee C H, Lian N T, Deng M C, Yang T H, Chen K C and Lu C Y 2007 *Semicond. Sci. Technol.* **22** 678
[52] Nickel N H, Johnson N M and Walker J 1995 *Phys. Rev. Lett.* **75** 3720
[53] Vuillaume D, Marchetaux J C and Boudou A 1991 *IEEE Electron Device Lett.* **12** 60
[54] Liu E K, Zhu B S and Luo J S 2007 *Semiconductor Physics* (Beijing: Beijing National Defense Industry Press) p 97
[55] Lui K M, Wong W H and Chik K P 1998 *Phys. Rev.* B **58** 16110
[56] Chik K P and Koon K C 1986 *Philos. Mag.* B **53** 399